Biointerface Research in Applied Chemistry
Open-Access Journal (ISSN: 2069-5837)

Article
Volume 13, Issue 3, 2023, 241
https://doi.org/10.33263/BRIAC133.241

Crystallite Shapes and Functional Data Analysis of Silk forms using X-ray Diffraction: Microwave Irradiation Effects

Gowtham Guttikatte Kariyappa [1,2], Thejas Gopal Krishne Urs [3,*], Manju Varanchi Venkata Shetty [4,*], Nandaprakash Mysore Basavaraju [5], Mahadeviah [6], Somashekarappa Hanumanthappa [2], Somashekar Rudappa[7]

1 Department of Physics, Shivagangotri, Davangere University, Davanagere, Karnataka – 577007; gowthamgk@live.com (G.G.K.);
2 Department of Physics, Yuvaraja's College, University of Mysore, Mysuru, India – 570005
3 Department of Physics, PES College of Engineering, Mandya, Karnataka – 577102; thejasursg@gmail.com (T.G.U.);
4 Department of Physics, Vidyavardhaka College of Engineering, Mysore, Karnataka – 570002; manjuvv@vvce.ac.in (M.V.V.);
5 Department of Physics, Karnataka State Open University, Mukthagangotri, Mysuru – 570006; nandaprakash_mb@rediffmail.com (N.M.B.);
6 Department of Polymer Science, Sir M.V PG Center, University of Mysore, Tubinkere, Mandya – 571402; mahadevupe@gmail.com (M.);
7 UPE Project, Center for Materials Science, University of Mysore, Vijnana Bhavan, Mysore, Karnataka – 570 006; rs@physics.uni-mysore.ac.in (R.S.);
* Correspondence: thejasursg@gmail.com (T.G.U.); manjuvv@vvce.ac.in (M.V.V.);

Scopus Author ID 57194472856
Received: 12.04.2022; Accepted: 17.05.2022; Published: 7.06.2022

Abstract: The silk cocoon of Bombyx mori, fiber, and thin films were considered in our study. The pure silk thin films were prepared by extracting silk from Bombyx mori cocoons. These samples were treated with microwave irradiation at different intervals, and X-ray diffraction data of these samples were obtained. XRD data of these samples were used as an essential input to compute crystallite size along with different Bragg reflections. Employing different statistical tools, the shape of the ordered region for different samples was obtained, and these shapes were analyzed and concluded that the obtained shapes are not ellipsoidal as assumed by earlier researchers and these are multi-shaped and strongly depend on the direction of Bragg reflections. The functional data analysis was also carried out to determine the correlation between physical and microstructural parameters.

Keywords: silk thin films; XRD; crystallite shapes; FDA; Polymer composite;

1. Introduction

Of all the fibrous materials, silk is a unique material because of its strength and luster. Many researchers around the world have been using silk as a suture material for centuries [1-7]. Studies on silk fibers have recently acquired attention as a biomaterial because of many attractive properties such as biocompatibility and excellent elasto-mechanical properties [8-12]. The Bombyx mori silk is basically made up of a protein of silk fibroin that is again coated with sericin protein. The adhesive protein sericin acquires the overall weight of cocoon silkworm for 25-30% [13]. The silk fibroin is made up of light and heavy chains; these are linked by a disulfide bond [14-17]. The crystalline-ordered regions of silk fibers are made up

of glycine-X repeats, where X indicates the amino acids such as alanine, serine, and valine [18]. Among these amino acids, the polar side chain is the region for forming amorphous regions. It is one of the co-polymers, composed of rich hydrophobic β-sheet-forming blocks that are connected by small hydrophilic spacers. The β-sheet arrangements within the fibroin structure give high elasto-mechanical strength and toughness to the fiber. It is fascinating to note that the irradiation process on fiber materials has significantly modified physical and microstructural properties that enhance fiber materials' physical properties [19]. The effect of radiation on materials has resulted in many interesting outcomes, which have attracted research interests from all disciplines. In light of this, an endeavor has been made to study the impact of microwave irradiation on the physicomechanical possessions of silk fibroin films; the developed silk fibroin films were illuminated for various dosage intervals and have analyzed samples utilizing X-ray diffraction techniques. In order to investigate the progressions in physical properties of these polymers, characterizations were carried out by X-ray diffraction studies. The crystallite shapes in 3-dimensions define the ordered regions in a material. Practically, crystallites typically have unpredictable and multi shapes, yet on normal, they may frequently be viewed as having a regular external form [20]. To analyse the effect of these ordered region on the physical and microstructural analogies, an attempt has been made to plot the probably ordered region in 3-dimensions for all the considered silk fibers. A new and novel method has been proposed [21-23], which can be extended to any material of interest. The functional data analysis technique (FDA) has been utilized to examine the estimations and dependence of a few micro-structural and macro-structural parameters of silk fiber films with some physical variables [24].

2. Materials and Methods

2.1. Sample preparation.

The raw and fresh silk cocoons were procured from the silk research institute, Central Sericultural Research and Training Institute (CSTRI), Mysuru, Karnataka, India. In order to obtain the fibroin core, these fibers were cleaned exhaustively and degummed in Na_2CO_3. The residual salt has been removed by washing it again. This fibroid core is dissolved in 9.3M LiBr solution as per the protocol of Rockwood *et al*. [25]. For three days, this solution was kept for dialysis, cast on the plate, and then silk films were prepared.2.2. Microwave irradiation.

To carry out the irradiation of studied silk films for different intervals, the domestic microwave has been utilized. The output power of this oven can be varied up to 700W by selecting the knob provided for this purpose. In our study, the power was kept to the medium position, i.e., 60%, 420W. The microwave irradiation was carried out for four different intervals, such as 10min, 20min, 30min, and 40min, respectively.

2.2. X-ray Diffraction studies.

Among all the available fibrous proteins, silk fibroin could seem to be the most reasonable for the determination of structure by the methods of X-ray diffraction technique. The X-ray crystallography study is the paramount source for discerning structural details [26, 27]. The Rigaku Denki Miniflex II Desktop Diffractometer has been utilized to carry out the XRD studies of silk fibers and silk films. The source of XRD was Cu-Kα with wavelength 1.5405 Å. The readings were noted down from 6 to 60 degrees with 0.02-degree intervals at

the speed of 5 degrees per minute at room temperature. Figure 1 indicates X-ray patterns for verities of silk and silk films.

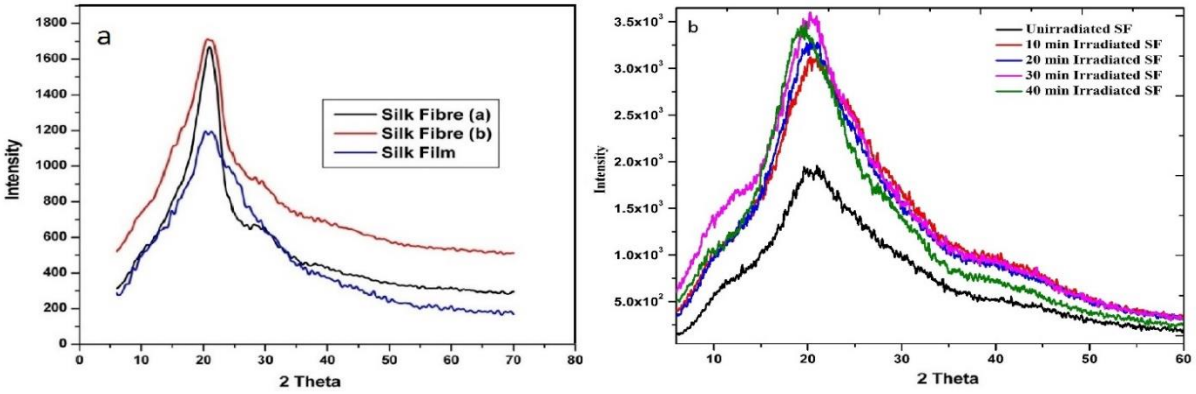

Figure 1. XRD recorded for the samples of polymer composite.

3. Results and Discussion

3.1. Determination of crystallite shapes for varieties of silk fiber and thin films.

The structure is an essential parameter for defining any material's microstructural and physical properties [28]. It is broadly acknowledged that structural parameters such as X-ray crystallinity, crystallite size, lattice strain, etc., are predominantly related to both chemical and physical properties of silk fibers such as elastic moduli, tensile strength, elongation, moisture content, etc. The XRD data of different silk films were used as a basic essential input for further analysis and some mathematical tools. The XRD data such as 2θ and intensity were used along with the Gaussian deconvolution method in peakfit® [29] software to simulate the obtained profile and separate the overlapping peaks. It is one of the sophisticated software that can be used for data manipulation purposes. The obtained Bragg reflections were additionally utilized in a numerical tool called checkcell® [23] to compute cell parameters and miller indices. Using the obtained reflections, FWHM, and 2θ values, the crystallite size for all the observed reflections was computed using the Debye Scherrer equation [30].

$$D_s = \frac{0.9 \times \lambda}{\beta \times cos(\theta)}$$

Here, Crystallite size is represented as D_s, the wavelength is $\lambda\ (1.54\text{Å}), \beta\ is\ FWHM$, and theta is the Bragg angle.

A program has been written in FORTRAN to obtain the spherical coordinates for the set of (hkl) and crystallite size values. We have three variables θ, ϕ, and Crystallite size (Ds) for all the reflections; these variables were plotted as a surface plot in Gnuplot available on Linux-based pc. The obtained crystallite size and lattice strain are shown in Table 1.

The figure origin addresses the point at which the X-ray beam hits the polymer film. From this origin, we have drawn a couple of Bragg reflection directions to show that crystallite shapes are not ellipsoids, which was accepted by some researchers in the advancement of mathematical models to comprehend the X-ray diffraction patterns from polymer samples [31].

Table 1. The computed crystallite size and strain for different samples.

Sample (SF Films)	Cocoon	Fiber	Film (Non-irradiated)	Irradiated for 10 minutes	Irradiated for 20 minutes	Irradiated for 30 minutes	Irradiated for 40 minutes
Crystallite Size in (Å)	33.20	34.46	40.8	44.8	49.7	63.5	95.8
% Lattice strain	2.3	3.6	4.7	5.7	6.3	6.9	7.5

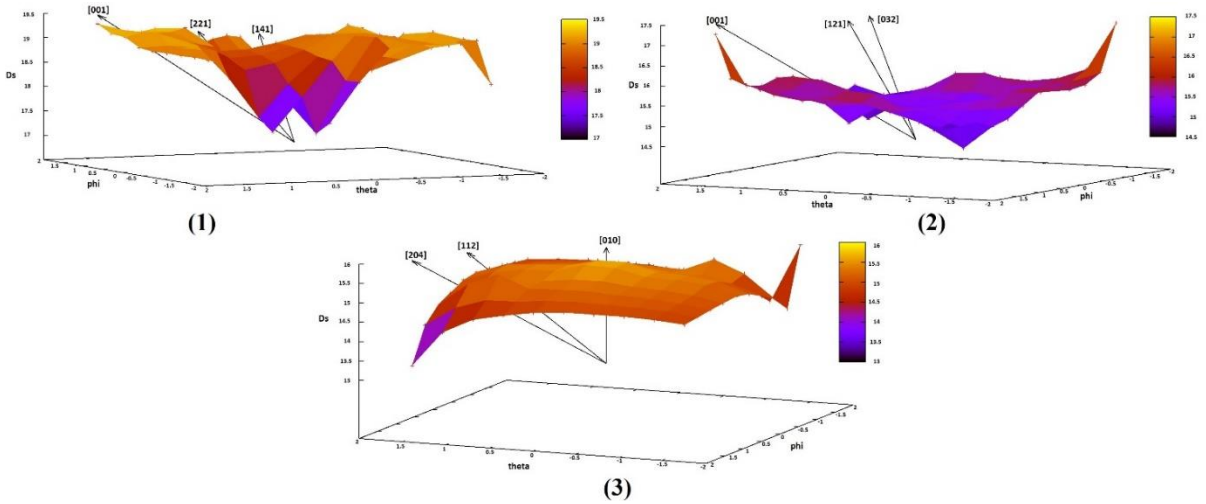

Figure 2. Shape of the ordered region obtained for (**1**) cocoon; (**2**) fiber; (**3**) film.

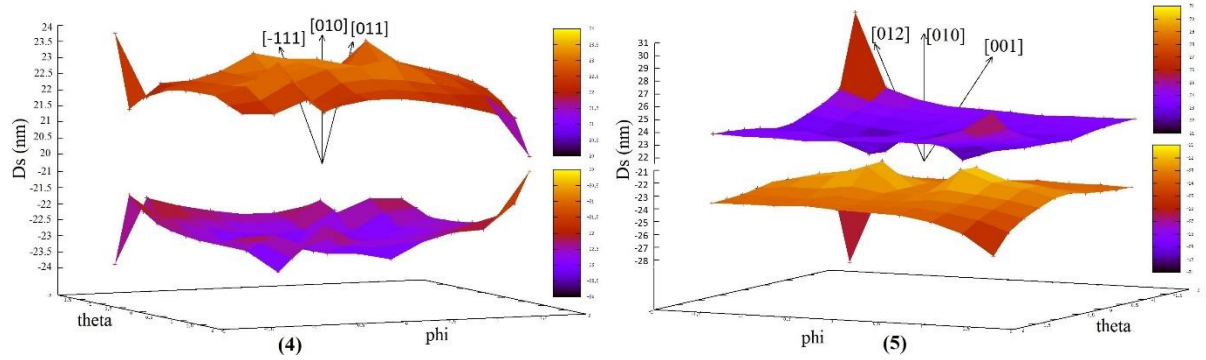

Figure 3. Shape of the ordered region obtained for microwave irradiated for (**4**) 10 mins; (**5**) 20 mins.

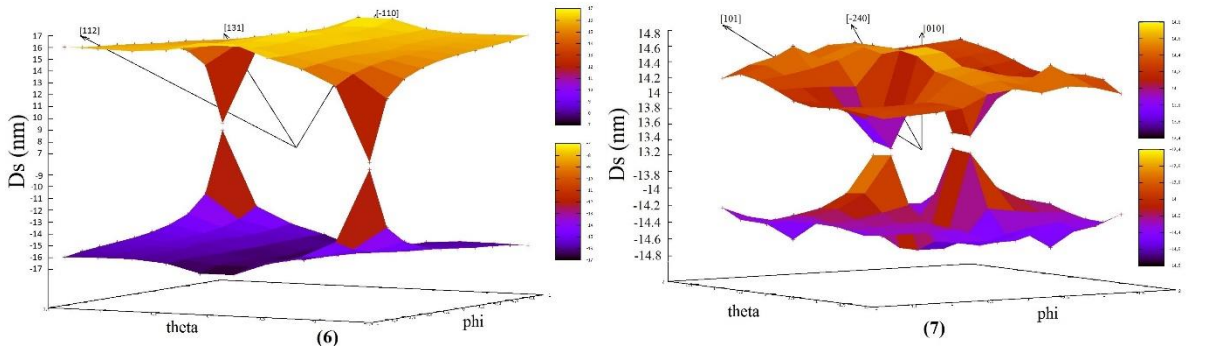

Figure 4. Shape of the ordered region obtained for microwave irradiated for (**6**) 30 mins; (**7**) 40 mins.

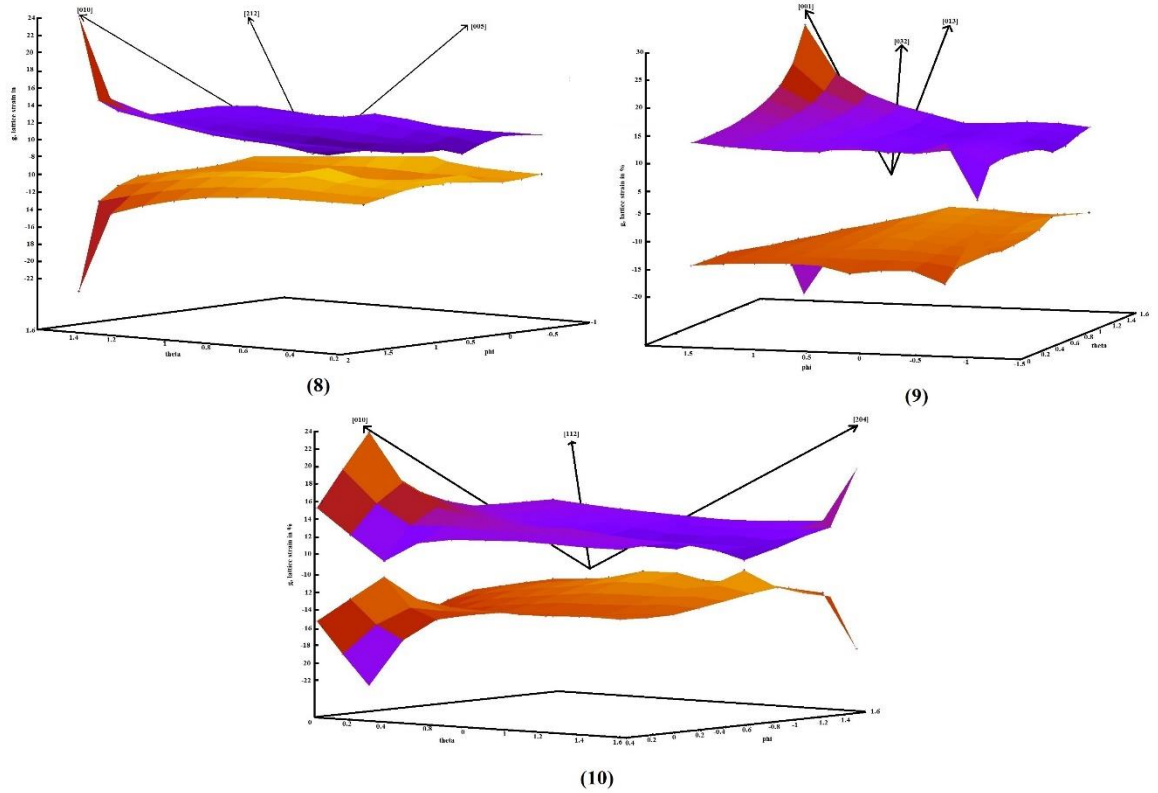

Figure 5. Shape of lattice strain obtained for (**8**) cocoon, (**9**) fiber, (**10**) film.

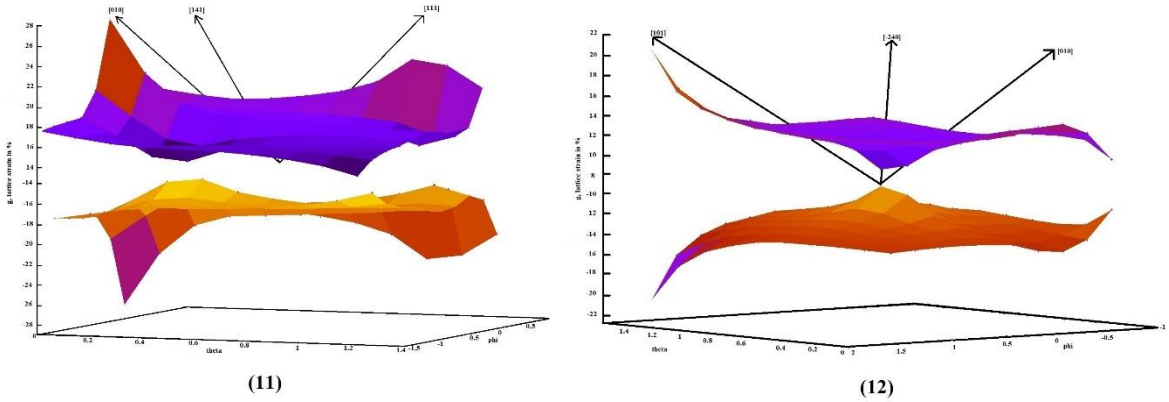

Figure 6. Shape of lattice strain (**11**) 10 mins microwave irradiation; (**12**) 20 mins microwave irradiation.

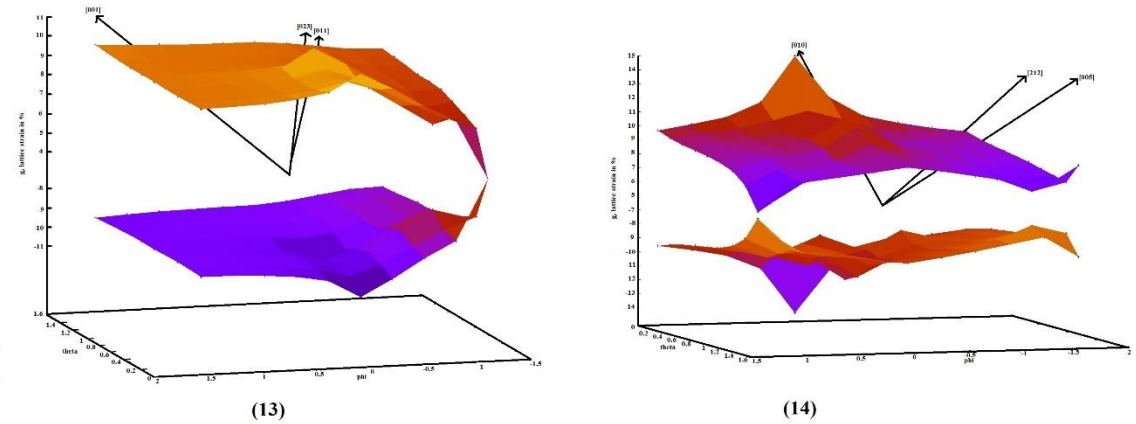

Figure 7. Shape of lattice strain (**13**) 30 mins microwave irradiation; (**14**) 40 mins microwave irradiation.

3.2. Functional data analysis.

The correlation functional analysis of the data is described here since there is no lucidity in the behavior of a few physicomechanical parameters for various dosage intervals. Let the value of θ observed at the j^{th} dosage value on the i^{th} trial be illustrated:

$$\theta_{ij} = \theta_i(t_j) + \epsilon_{ij} = \mu(t_{ij}) + \sum_{k=1}^{\infty} \xi_{ik} \ \Phi_k(t_{ij}) + \epsilon_{ij}$$

$$\approx \mu(t_{ij}) + \sum_{k=1}^{M} \xi_{ik} \ \Phi_k(t_{ij}) + \epsilon_{ij}$$

where ϵ_{ij} are random experimental fallacy. The mean function has been obtained by solving the optimization problem:

$$\hat{\mu}(t) := \operatorname{argmin}_{f \in F} \sum_{i=1}^{n} \sum_{j=1}^{n_i} (\theta_{ij} - f(t_{ij}))^2 + \lambda \int_{\mathbb{R} \geq 0} (f''(t))^2 dt,$$

where F is the class of square intergrable function.

The freely available FPCA package has been utilized to compute the above relations. Here the objective is to capture correlations between parameters as a component of dosages. The functions defined in the above conditions are of the orthonormal premise, and eigenfunctions of the covariance operator that can be assessed effectively utilizing the FPCA package. We utilize the eigenfunctions straightforwardly to plot and envision relationships. Here we recreate the correlation surface for crystallite size and strain. From these eigenvalues, we obtain the mean value of the physical parameters, and they are given in Figure 8 and Figure 9. These values are used to compute the material's performance index exposed for different dosages.

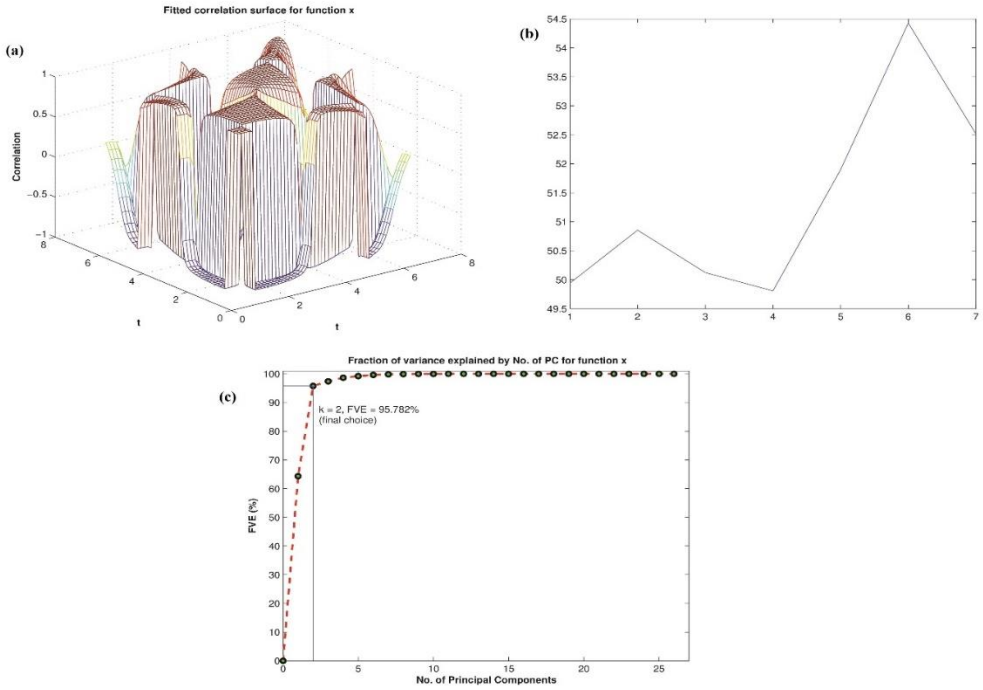

Figure 8. (**a**) Surface correlation of crystallite size; (**b**) mean crystallite size; (**c**) variation of the principal component.

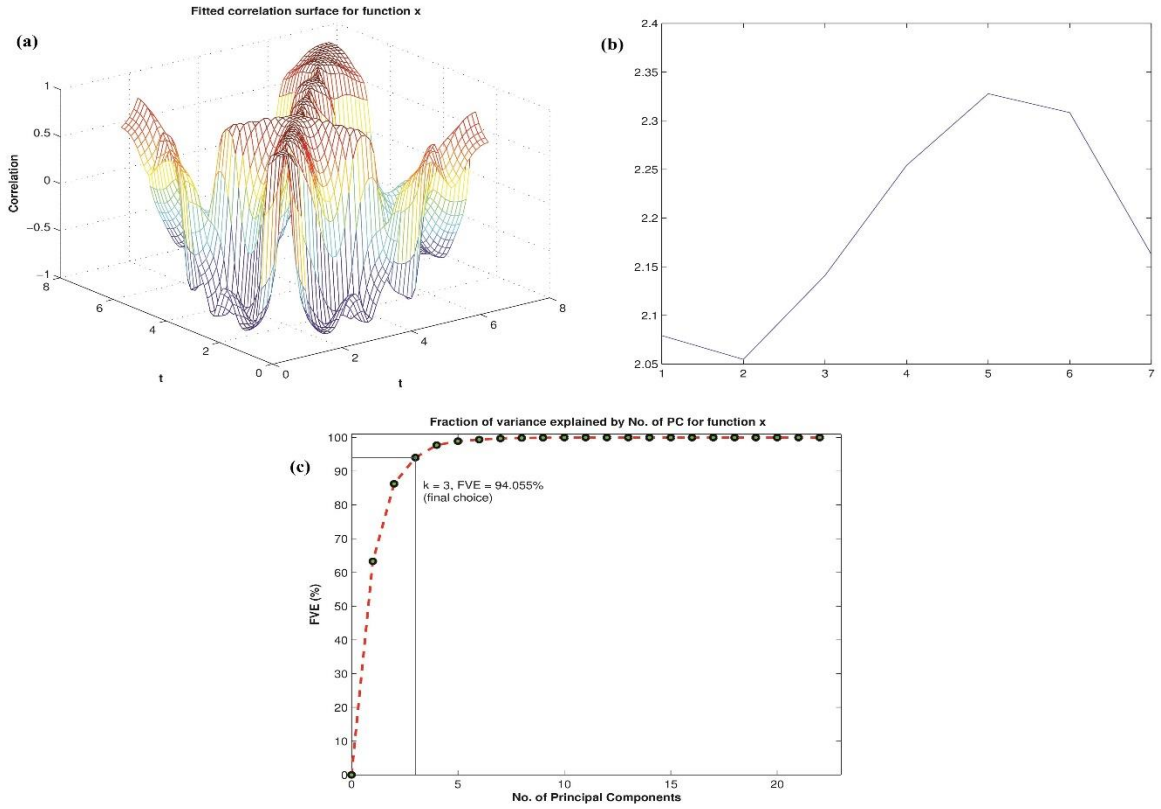

Figure 9. (**a**) Surface correlation of crystallite strain; (**b**) mean crystallite strain; (**c**) variation of the principal component.

PMS is a multivoltine Bombyx mori fiber, and for all practical purposes, it was considered amorphous. It is obvious from the study outcomes that there is a formation of strong polypeptide chains due to microwave irradiation. This method persuaded cross-linking among the amide groups. This solid reordering of the silk chain secludes the particles of interstitial lithium [32, 33] in the lattice, which was available as a debasement even after dialysis. Microwave illumination gives rise to the clear recognition of such remanent lithium particles. Also, it is evident that there is an improvement in the crystalline regions of silk films when exposed to microwave radiation. This suggests an increase in the cross-linking of polypeptides in the beta-pleated structure and hence in the strength of the films. This is readily seen in the raw X-ray recordings, wherein the pristine silk fibroin film showed a broad but less intense diffraction profile. With irradiation, these films showed a sharper profile with less FWHM value.

The computation of crystallite shape in a cocoon, fiber, and film of PMS silk and they are all having different shapes. The origin of the shape given in the figures signifies the point at which the X-ray strikes the sample [34]. From this point along any Bragg direction, the crystallite shape and size for all the three forms and their figures have been reported for the first time here. Crystallite shapes computed for the studied varieties of samples are represented in Figures 2 to 7. Put together from the obtained reflections and their corresponding (hkl) values, and these crystallite shapes differ from one another. From the figures, the observed Bragg reflections for silk cocoon, fiber, and film, it is clear that along [001], [001], and [010], respectively, depict the maximum crystallite surface gradient [35, 36]. This is due to the rearranging of the β pleated structure in all forms of silk [37].

4. Conclusions

Re-crystallization to form silk film is associated with a very small amount of remanent lithium ions in the polymer network occupying interstitial sites. The effect of microwave irradiation on films of silk fibroin improves the arrangement of the polypeptide chain. Subsequently, it supports the recovery of silk fibroin formation as a stable thin film. Additionally, such recovery of silk fibroin prompts the confinement of remaining lithium particles, formerly interstitial. Thus, microwave irradiation facilitates silk fibroin protein to reclaim its structure and physical properties; it is to be noted that the energy is not sufficient to change the preliminary structure of the polypeptide alignments in the unit cell. The statistically analyzed results also show this variation trend and support the analysis. From the obtained shapes, it is seen that there are notable differences among the considered systems. Accordingly, such variations in the crystallite shapes can be ascribed to clarifying the sub-atomic interactions and structure formations. Functional data analysis has given a vigorous technique for extracting the correlation between physical properties and silk, fiber, and silk thin-film assortments by portraying the dependence of actual properties on the microstructural parameters.

Funding

This research received no external funding.

Acknowledgments

The authors would like to thank UGC for UPE & CPEPA projects for the University of Mysore.

Conflicts of Interest

The authors declare no conflict of interest.

References

1. Júnior, E.; Neves, F.B.; Lopes, S.Q.; Holanda, F.H.; Souza, T.M.; Pinto, E.P.; Oliveira, A.N.; Fonseca, L.P.; Yoshioka, S.A.; Ferreira, I.M. Immobilization of Amano AK lipase from Pseudomonas fluorescens on novel silk microfiber using Oxone®: parameter optimization for enzymatic assays and use in esterification of residual palm oil. *Current Catalysis* **2021**, *10*, 119-129, https://doi.org/10.2174/2211544710666210401111704.
2. Jamshaid, H.; Mishra, R.; Hussain, U.; Rajput, A.W.; Tichy, M.; Muller, M. Natural Fiber Based Antibacterial, Wound Healing Surgical Sutures by the Application of Herbal Antimicrobial Compounds. *Journal of Natural Fibers* **2021**, *18*, 1-16, https://doi.org/10.1080/15440478.2021.1988798.
3. Liu, Z.; Xia, L.; Ke, H.; Zou, L. Effect of Silk Sericin Content on the Electrospun Silk Nanofibrous Membrane Property. *Micro and Nanosystems* **2021**, *13*, 67-73, http://dx.doi.org/10.2174/1876402912666200319152508.
4. Zhang, Y.; Ye, S.; Cao, L.; Lv, Z.; Ren, J.; Shao, Z.; Yao, Y.; Ling, S. Natural Silk Spinning-Inspired Meso-Assembly-Processing Engineering Strategy for Fabricating Soft Tissue-Mimicking Biomaterials. *Advanced Functional Materials* **2022**, 2200267, https://doi.org/10.1002/adfm.202200267.
5. Qing, C.; Li, Q.-y.; Xue, N.-n.; Yuan, S.-m.; Liu, C.-j.; Zhang, C.-g.; Li, H.-w.; Zhao, Y. The Outlook of the Development of Innovative Products from Biocompatible Natural Spider Silk in the Beauty Thread-Lifting Industry. *Natural Products and Bioprospecting* **2021**, *11*, 21-30, https://doi.org/10.1007/s13659-020-00291-9.
6. Sammi, A.; Mahapatra, S.; Kumar, R.; Chandra, P. Nano-Bio-Engineered Silk Matrix based Sensing Devices for Molecular Bioanalysis. *Authorea* **2021**, https://doi.org/10.22541/au.163542733.35988534/v1.

7. Zhao, M.; Qi, Z.; Tao, X.; Newkirk, C.; Hu, X.; Lu, S. Chemical, thermal, time, and enzymatic stability of silk materials with silk i structure. *International journal of molecular sciences* **2021**, *22*, 4136, https://doi.org/10.3390/ijms22084136.
8. Guo, P.; Du, P.; Zhao, P.; Chen, X.; Liu, C.; Du, Y.; Li, J.; Tang, X.; Yang, F.; Lv, G. Regulating the mechanics of silk fibroin scaffolds promotes wound vascularization. *Biochemical and Biophysical Research Communications* **2021**, *574*, 78-84, https://doi.org/10.1016/j.bbrc.2021.08.026.
9. Malekmohammadi, S.; Sedghi Aminabad, N.; Sabzi, A.; Zarebkohan, A.; Razavi, M.; Vosough, M.; Bodaghi, M.; Maleki, H. Smart and Biomimetic 3D and 4D Printed Composite Hydrogels: Opportunities for Different Biomedical Applications. *Biomedicines* **2021**, *9*, 1537, https://doi.org/10.3390/biomedicines9111537.
10. Lai, H.; Xiao, P. Main challenges in 3D printing: Printing speed and biomedical applications. In: *3D Printing with Light* **2021**, De Gruyter, https://doi.org/10.1515/9783110570588-010.
11. Laomeephol, C.; Vasuratna, A.; Ratanavaraporn, J.; Kanokpanont, S.; Luckanagul, J.A.; Humenik, M.; Scheibel, T.; Damrongsakkul, S. Impacts of Blended *Bombyx mori* Silk Fibroin and Recombinant Spider Silk Fibroin Hydrogels on Cell Growth. *Polymers* **2021**, *13*, 4182, https://doi.org/10.3390/polym13234182.
12. Molinnus, D.; Drinic, A.; Iken, H.; Kröger, N.; Zinser, M.; Smeets, R.; Köpf, M.; Kopp, A.; Schöning, M.J. Towards a flexible electrochemical biosensor fabricated from biocompatible Bombyx mori silk. *Biosensors and Bioelectronics* **2021**, *183*, 113204, https://doi.org/10.1016/j.bios.2021.113204.
13. Reddy, R.; Jiang, Q.; Aramwit, P.; Reddy, N. Litter to leaf: The unexplored potential of silk byproducts. *Trends in Biotechnology* **2021**, *39*, 706-718, https://doi.org/10.1016/j.tibtech.2020.11.001.
14. Lee, S.; Kim, S.H.; Jo, Y.-Y.; Ju, W.-T.; Kim, H.-B.; Kweon, H. Effects of ultraviolet light irradiation on silk fibroin films prepared under different conditions. *Biomolecules* **2021**, *11*, 70, https://doi.org/10.3390/biom11010070.
15. Hao, Z.; Long, D.; Zhang, Y.; Umuhoza, D.; Dai, J.; Xu, Z.; Zhang, G.; Meng, W.; Xiang, Z.; Zhao, A. New insight into the mechanism of *in vivo* fibroin self-assembly and secretion in the silkworm, *Bombyx mori*. *International Journal of Biological Macromolecules* **2021**, *169*, 473-479, https://doi.org/10.1016/j.ijbiomac.2020.12.132.
16. Prakash, N.J.; Mane, P.P.; George, S.M.; Kandasubramanian, B. Silk Fibroin As an Immobilization Matrix for Sensing Applications. *ACS Biomaterials Science & Engineering* **2021**, *7*, 2015-2042, https://doi.org/10.1021/acsbiomaterials.1c00080.
17. Vallejo-Martinez, M.; Puerta, M.; Restrepo-Osorio, A. Electrospun silk fibroin using aqueous and formic acid solutions. *MRS Advances* **2021**, *6*, 975-979, https://doi.org/10.1557/s43580-021-00192-0.
18. Pei, X.; Wang, J.; Cong, Y.; Fu, J. Recent progress in polymer hydrogel bioadhesives. *Journal of Polymer Science* **2021**, *59*, 1312-1337, https://doi.org/10.1002/pol.20210249.
19. Yan, B.; Bao, X.; Liao, X.; Wang, P.; Zhou, M.; Yu, Y.; Yuan, J.; Cui, L.; Wang, Q. Sensitive Micro-Breathing Sensing and Highly-Effective Photothermal Antibacterial Cinnamomum camphora Bark Micro-Structural Cotton Fabric via Electrostatic Self-Assembly of MXene/HACC. *ACS Applied Materials & Interfaces* **2022,** *14*, 2132-2145, https://doi.org/10.1021/acsami.1c22740.
20. Šimonová, P.; Pabst, W.; Cibulková, J. Crystallite size of pure tin oxide ceramics and its growth during sintering determined from XRD line broadening–A methodological case study and a practitioners' guide. *Ceramics International* **2021**, *47*, 35333-35347, https://doi.org/10.1016/j.ceramint.2021.09.076.
21. Akinyemi, B.A.; Adesina, A. Utilization of polymer chemical admixtures for surface treatment and modification of cellulose fibres in cement-based composites: a review. *Cellulose* **2021**, *28*, 1241-1266, https://doi.org/10.1007/s10570-020-03627-3.
22. Manju, V.; Divakara, S.; Somashekhar, R. Comparison of crystallite shapes in four different varieties of cotton fibers using X-ray powder diffraction data. *AIP Conference Proceedings* **2017**, *1832*, 040013, https://doi.org/10.1063/1.4980215.
23. Manju, V.; Thejas Gopal, Urs; Diavakara, S; Somashekar, R. Imaging of crystalline regions in cotton fibers using powder XRD. Foundations of Crystallography 2017, 70, C564.
24. Urs, T.G.K.; Bharath, K.; Yallappa, S.; Rudrappa, S. Functional data analysis techniques for the study of structural parameters in polymer composites. *Journal of Applied Crystallography* **2016**, *49*, 594-605, https://doi.org/10.1107/S1600576716003113.
25. Casanova, E.; Santiago, C.; Guerra, A.J.; Ciurana, J. High Concentrated Silk Based Bioink For 3d Printing–Design Parameters. In *Conference of Pre-doctoral Researchers* **2021**, *3*, 133-136.

26. Schaffer, J.E.; Kukshal, V.; Miller, J.J.; Kitainda, V.; Jez, J.M. Beyond X-rays: an overview of emerging structural biology methods. *Emerging Topics in Life Sciences* **2021**, *5*, 221-230, https://doi.org/10.1042/ETLS20200272.
27. Smyth, M.; Martin, J. xRay crystallography. *Molecular Pathology* **2000**, *53*, 8, http://dx.doi.org/10.1136/mp.53.1.8.
28. Manju, V.V.; Hegde, V.N.; Divakara, S.; Somashekar, R. Comparison of structural and mechanical properties of suvin and MCU-5 cotton fibres. *Advances in Materials and Processing Technologies* **2021**, 1-15, https://doi.org/10.1080/2374068X.2021.1878697.
29. Chen, R.; Jakes, K.A.; Foreman, D.W. Peak-fitting analysis of cotton fiber powder X-ray diffraction spectra. *Journal of Applied Polymer Science* **2004**, *93*, 2019-2024, https://doi.org/10.1002/app.20666.
30. Monshi, A.; Foroughi, M.R.; Monshi, M.R. Modified Scherrer equation to estimate more accurately nano-crystallite size using XRD. *World J Nano Sci Eng* **2012**, *2*, 154-160, http://dx.doi.org/10.4236/wjnse.2012.23020.
31. Manju, V.V.; Divakara, S.; Narayan Hegde, V.; Somashekar, R. Structural and Elastic Properties of Varieties of Cotton Fibers. *Advances in Materials and Processing Technologies* **2022**, 1-17, https://doi.org/10.1080/2374068X.2022.2036502.
32. Rockwood, D.N.; Preda, R.C.; Yücel, T.; Wang, X.; Lovett, M.L.; Kaplan, D.L. Materials fabrication from *Bombyx mori* silk fibroin. *Nature Protocols* **2011**, *6*, 1612-1631, https://doi.org/10.1038/nprot.2011.379.
33. El-Aswar, E.I.; Ramadan, H.; Elkik, H.; Taha, A.G. A comprehensive review on preparation, functionalization and recent applications of nanofiber membranes in wastewater treatment. *Journal of Environmental Management* **2022**, *301*, 113908, https://doi.org/10.1016/j.jenvman.2021.113908.
34. Konovalov, O.V.; Belova, V.; La Porta, F. *et al*. X-ray reflectivity from curved surfaces as illustrated by a graphene layer on molten copper. *Journal of Synchrotron Radiation* **2022**, *29*, 711-720, https://doi.org/10.1107/S1600577522002053.
35. Chen, J.; Tsuchiya, K.; Masunaga, H.; Malay, A.D.; Numata, K. A silk composite fiber reinforced by telechelic-type polyalanine and its strengthening mechanism. *Polymer Chemistry* **2022**, *13*, 1869-1879, https://doi.org/10.1039/D2PY00030J.
36. Patil, S.P.; Kulkarni, A.; Markert, B. Mechanical Properties of Dragline Silk Fiber Using a Bottom-Up Approach. *Journal of Composites Science* **2022**, *6*, 95, https://doi.org/10.3390/jcs6030095.
37. Wang, K.; Ma, Q.; Zhou, H.-T.; Zhao, J.-M.; Cao, M.; Wang, S.-D. Review on Fabrication and Application of Regenerated Silk Fibroin Materials. *Autex Research Journal* **2022**, https://doi.org/10.2478/aut-2021-0059.